Adaptive imaging spectrometer in a time-domain filtering architecture

Yang Jiao, Sameer R. Bhalotra, Helen L. Kung, and David. A. B. Miller

Edward L. Ginzton Laboratory
Stanford University, Stanford, CA 94305-4088
jiaoyang@stanford.edu, sbhalotra@yahoo.com, hlkung@stanfordalumni.org, dabm@ee.stanford.edu

Abstract: We demonstrate an imaging spectrometer with 30nm resolution that utilizes a novel time-domain filtering architecture. The architecture is based on a pixel by pixel integration of the interferogram signal mixed with reference waveforms. The system can be adapted in real time to discriminate between LED sources of different wavelengths, perform signal processing on the spectra, as well as discriminate between highly overlapping, broadband spectral features in a scene illuminated by a tungsten lamp. Unlike a conventional spectral signature discrimination system, which needs a dedicated computation subsystem running a discrimination algorithm, the time-domain filtering architecture embeds much of the computation in the filtering, which will aid the design of integrated miniaturized spectral signature discrimination systems.

©2003 Optical Society of America

OCIS codes: (300.6190) Spectrometers; (300.6300) Fourier transforms; (350.5730) Resolution.

References and Links

1. R.J. McNichols, G.L. Coté, "Optical glucose sensing in biological fluids," J. Biomed. Opt. **5**, 5 (2000).
2. N. Gupta, R. Dahmani, "Multispectral and hyperspectral imaging with AOTF for object recognition," Proc. SPIE **3584**, 128 (1999).
3. H. L. Kung, S. R. Bhalotra, J. D. Mansell, D. A. B. Miller, and J. S. Harris, Jr., "Standing-wave transform spectrometer based on integrated MEMS mirror and thin-film photodetector," IEE J. Sel. Top. Quantum Electron. **8,** 98-105 (2002).
4. S. R. Bhalotra, H. L. Kung, Y. Jiao, and D. A. B. Miller, "Adaptive time-domain filtering for real-time spectral discrimination in a Michelson interferometer," Opt. Lett. **27**, 1147-1149 (2002).
5. R. E. Shaffer, R. J. Combs, "Comparison of spectral and interferogram processing methods using simulated passive Fourier transform infrared remote sensing data," Appl. Spectrosc. **55**, 1404-1413 (2001).
6. A. S. Banalore, G. W. Small, R. J. Combs, R. B. Knapp, R. T. Kroutil, C. A. Traynor, J. D. Ko, "Automated detection of trichloroethylene by Fourier transform infrared remote sensing measurements," Anal. Chem. **69**, 118-129 (1997).
7. P. O. Idwasi, G. W. Small, R. J. Combs, R. B. Knapp, R. T. Kroutil, "Multiple filtering strategy for the automated detection of ethanol by passive Fourier transform infrared spectrometry," Appl. Spectrosc. **55**, 1544-1552 (2001).
8. J. W. Childers, W. J. Phillips, E. L. Thompson Jr., D. B. Harris, D. A. Kirchgessner, D. F. Natschke, M. Clayton. "Comparison of an innovative nonlinear algorithm to classical least-squares for analyzing open-path Fourier transform infrared spectra collected at a concentrated swine production facility," Appl. Spectrosc. **56**, 325-335 (2002).
9. R. A. DeVerse, R. M. Hammaker, and W. G. Fateley, "Realization of the Hadamard multiplex advantage using a programmable optical mask in a dispersive flat-field near-infrared spectrometer," Appl. Spectrosc. **54**, 1751 (2000).
10. J. Proakis and M. Salehi, *Communication Systems Engineering*. (Prentice Hall, New York, 1994).

Miniaturized spectral signature discrimination systems have important applications in remote sensing and medical diagnosis (see, e.g., Refs. [1,2]). A conventional spectral signature discrimination system is typically comprised of two subsystems: an optical-to-electrical

sensing front-end with both optical and electrical filtering, and a separate subsystem executing a discrimination algorithm. In recent years, microfabrication has enabled the miniaturization of the sensing front-end [3]. However, the discrimination algorithm is often too computationally demanding to integrate into the sensing front-end, which prevents straightforward integration and miniaturization of the whole spectral signature discrimination system. To address this problem, we present a novel time-domain filtering (TDF) architecture. The architecture greatly simplifies the discrimination algorithm by utilizing a bank of filters to process the spectral data in the sensing front-end. Ease of integrating the filter bank with the sensing front-end means that, effectively, much of the computation for discrimination is embedded in the sensing front-end. Ultimately, the TDF architecture will aid in the design of an integrated miniaturized spectral signature discrimination system.

We have previously briefly introduced the concept of TDF in a proof of principle experiment discriminating laser wavelengths [4]. In this paper, we show the power and flexibility of the concept in working with images and with low coherence light, while preserving the ability to discriminate features of interest, through two experiments. First, we show real-time discrimination of multiple LED spectra in an image using a TDF system. To demonstrate the signal-processing capabilities of the architecture, the system is modified slightly to perform real-time enhancement of individual LED spectra while suppressing combinations of the same spectra (a function that a conventional color camera cannot perform). In the second experiment, using the same simple low-resolution system, but adding one elementary computation step, the system is used to discriminate between highly overlapping broadband spectra in real time.

Spectral signature detection using digitally filtered interferograms in a Fourier transform spectrometer (FTS) has been demonstrated previously, and yields performance comparable to data analysis of conventional spectra [5,6]. Just like conventional spectral analysis, however, significant processing is still needed after interferogram filtering to obtain the result of the discrimination [7,8]. The TDF system demonstrates that time domain filtering could share much more of the processing burdens of the discrimination. For each pixel of the scene, the TDF system records a time-varying measurement waveform $I_{x,y}$. $I_{x,y}$ is then multiplied by a time-varying reference waveform R, and the result is integrated, i.e., one computes the inner product of $I_{x,y}$ and R. The inner product can be used to deduce how close $I_{x,y}$ is to the spectral signatures, even if the signatures greatly overlap. By choosing the appropriate reference waveform R or a set of reference waveforms $R_1,...,R_n$, the output could directly indicate the presence of the spectral signatures. Note that, because the desired result is an inner product, it is not necessary to transform to any particular basis (e.g., Fourier transform), because the inner product is independent of the basis used. This way, for target spectral signatures that may contain the spectral signature of interest, the TDF architecture skips the decomposition of the scene into separate wavelength bins, and directly extracts the spectral signatures at a very early stage of the physical sensing process.

The key advantages of TDF over traditional multispectral imager architectures are elaborated in [4]. Compared to FTS, only one single data value per pixel per reference waveform is generated instead of an entire sampled interferogram. For a small number of references, this presents a significant reduction in the amount of data to be transmitted and processed. TDF eliminates the need for Fourier transforms. It also compensates for scan-nonlinearities in the interferogram acquisition, as long as the nonlinearities remain constant from pixel to pixel. In fact, the method can be used with any linear transform of the input optical signal, including, e.g., Fourier and Hadamard [9] transforms, and other transforms such as that performed by a Fourier transform spectrometer configuration with a sinusoidal (rather than linear) scan of the mirror [3]. Furthermore, by embedding the signal analysis in the reference waveform, the systems can switch on-demand between various signal processing and spectral signature extraction functions by changing the reference waveforms. Since the reference waveforms may be stored electronically and selected under simple software control, no hardware reconfiguration is needed.
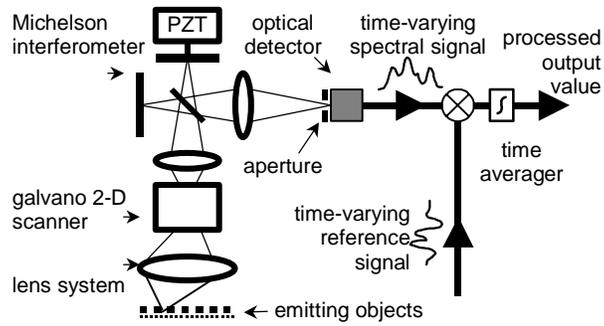
Fig. 1. Time-domain filtering setup.

We demonstrate TDF in two experiments, both with the same physical setup shown in Fig. 1. A lens system collects light from a point in the scene. This light is focused into a 2-D raster scan galvano mirror set, which steers the light beam into a Michelson interferometer. A piezoelectric transducer (PZT) actuator varies the path length from 0μm to 13μm in one interferometer arm. To demonstrate the system's insensitivity to scan nonlinearity, the PZT is driven by a 30 Hz DC-offset sinusoid rather than the linear scan required by a conventional FTS. Sinusoidal scans can be much easier to produce in practice than linear scans, allowing the use of mechanically resonant systems that can give large displacement for small drives [3]. The interferogram for each pixel is converted to an electrical waveform by an amplified Si photodetector (PD). The PD is 0.9mm in diameter with a 0.5mm aperture. After amplifying the PD signal and filtering out the DC drift and the high frequency noise, the raw interferogram signal is recorded by a computer (PC). To average the detector pre-amplifier noise, the interferogram is recorded for 3 periods of the PZT scan for each pixel. The PZT actuation, raster scanning, and data acquisition are controlled and synchronized by the PC.
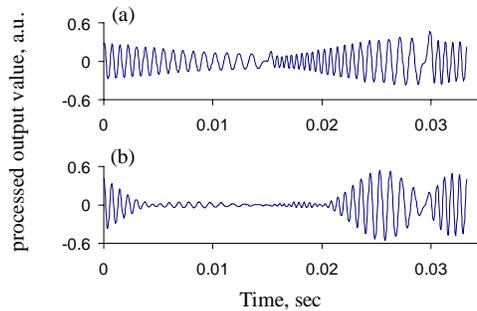

Fig. 2. Example reference interferograms. (a) is the reference interferogram recorded with a yellow LED, and (b) is the interferogram formed by taking the difference of the interferograms of the red and green LEDs

In the first experiment, we demonstrate TDF's abilities to discriminate multiple LED spectra, and enhance individual LED spectra while suppressing combinations of the same spectra. We obtain reference waveforms by recording the interferogram from sources with the desired spectral signatures. Because of the non-linear scanning of the interferometer arms and the short scan length, the interferogram is not an accurate inverse FT of the spectral signature. Recording the reference waveforms from known sources takes care of the scan nonlinearities, in contrast to a conventional FTS, which requires an exactly linear scan in time or compensation of the scan nonlinearity. For this demonstration, the PC calculates the inner product between the interferogram and the recorded reference waveforms. This multiplication task can also be performed by simple analog circuitry [4] or even as a part of the sensing front-end (e.g., by modulating the detector response with the reference function); the PC is

used here for flexibility in performing and analyzing different experiments. We emphasize that, in this TDF approach, only a simple multiplication of the signal and reference, followed by integration or averaging, is required; no transforms have to be performed on the signals.

We obtain three reference waveforms R_{red}, R_{yellow}, and R_{green} by recording the interferograms from red, yellow, and green LEDs respectively (e.g., Fig. 2(a)). We also utilize an inhibitory reference waveform $R_s = aR_{red} - bR_{green}$, where a, b are weighting factors (Fig. 2(b)). The inhibitory reference waveform suppresses the output when the red and green spectral signatures are present simultaneously in a ratio determined the factors a and b, but will generate an output signal when either one of the spectral signatures is present alone. Expansion to a parallel analysis with more than 4 reference waveforms is trivial, requiring only additional software or hardware multiplication and integration channels.

Figure 3 shows the object imaged by a conventional color camera with annotation of the LED colors. The two-color LEDs in the middle row simultaneously emit both red and green light. Figures 3(b), (c), and (d) show the spectrometer output after applying R_{red}, R_{yellow}, and R_{green}. Even though the ratio of the red and green intensities in the two-color LEDs are adjusted so that their visually perceived color is indistinguishable from the true yellow LED, the two-color LEDs correctly appear in both green and red channels but are substantially suppressed in the yellow channel. The system separates the red and green spectral signatures in Figs. 3(b) and (c), distinguishing also the true yellow and the apparent yellow of the red-green mixture. Spectral overlap caused some cross-talk between the yellow and green discriminations. We define the spectral resolution, $\Delta\nu$, as the FWHM of the impulse response of the FTS. It is straightforward to shown, based on a Rayleigh resolution criterion, that $\Delta\nu = 1.206 * c/L$, where L is the interferometer scan length and c is the speed of light. The yellow and green spectral peaks are 30 nm apart, which is the nominal spectral resolution limit theoretically obtainable from a 13 μm interferogram, and leads to only partial discrimination between green and yellow spectral signatures. As we will show later in this letter, by using more sophisticated reference waveforms, discrimination is still possible below $\Delta\nu$.

The result of applying the inhibitory reference waveform (Fig. 2(b)) is shown in Fig. 3(e). The shading is black (negative) for red-only spectra, white (positive) for green-only spectra, and gray for no spectra or red-green combined spectra. The signals from the two-color LEDs are suppressed when the red and green signatures appear in the same pixel. The resulting image had drastically enhanced contrast between the two-color LEDs and the single-color LEDs. With a single detector with no intrinsic color sensitivity, we are able to discriminate multiple colors and additive or inhibitory combinations of colors with this approach.
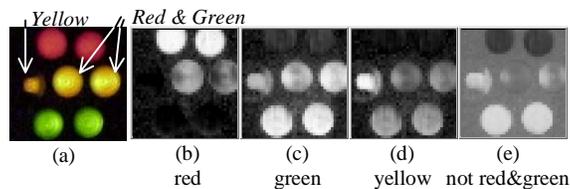

Fig. 3. 40X40 pixel images of the object. a) shows the conventional color camera image. b), c) and d) show the overlap integral of each pixel's interferogram with the reference waveforms red, green, and yellow respectively. White areas indicate the presence of a spectral signature. e) shows the overlap integral with the reference "not red&green". Areas that only contain a green component are white; red is dark, gray areas contain either both or none of the spectral signatures. The incomplete mixing of the light from the two LEDs within each two-color LED causes the in-homogeneity of the two-color LED image.

The yellow and green LED spectra peaks are barely resolvable because of the limited spectral resolution of the underlying Michelson interferometer. Because TDF does not rely on decomposing each pixel into intensities for an array of frequency bins, the spectral resolution

limit of the underlying interferometer can actually be circumvented in detection applications, as we will demonstrate in our second experiment with TDF.

For experiment two, we modify TDF slightly to discriminate between 4 highly overlapping spectral signatures. The modification is chosen because of its hardware implementation simplicity. The same architecture also enables discrimination of spectral lines with a separation smaller than the spectral resolution of the underlying FTS. We will refer to this modified discrimination system as the as the maximum-likelihood (ML)-TDF system.

In ML-TDF, we also start by recording R_1, … , R_4. Using Gram-Schmitt orthogonalization [10], we find the vector space S spanned by R_1, … , R_4. We assume that the noise in the measurement waveforms is additive white Gaussian, and that each spectral signature is equally likely to be the source of $I_{x,y}$. Then, instead of finding the correlation between R_i and $I_{x,y}$, we project $I_{x,y}$ into S for each location (x,y), compute the Euclidean distance between the projection and R_1, … , R_n, and pick the R_i closest to $I_{x,y}$ as the most likely dominating spectrum at location (x,y). It should be noted that the set of basis vectors found by Gram-Schmitt orthogonalization is not unique. ML-TDF works with basis vectors generated with any orthogonalization procedure. The choice of the optimal set of basis vectors depends on the reference waveforms and the type of noise, a topic left for future work.

The physical setup of ML-TDF and TDF are identical. In ML-TDF, projection of $I_{x,y}$ into S does not require any change to TDF, since the projection is performed by taking the inner product of $I_{x,y}$ with the basis waveforms of S. The only additional computation needed for each pixel is comparing the Cartesian distances between $I_{x,y}$ and R_1, … , R_n (considering these as vectors in a multidimensional space). This is a simple enough operation that it could be performed with analog circuitry, though here we use the PC for convenience. In this architecture demonstration, the PC is responsible for the ML discrimination and finding S.

We use ML-TDF to examine the scene shown in Fig. 4(a). The scene is a color printout illuminated by a tungsten lamp. The letters A, B, C in the scene and the rectangles underneath give red, green, and yellow spectral signatures respectively (Fig. 5). The black background also has a specific spectral signature because of its non-zero reflection. R_1, … , R_4 are obtained by measuring spectral signatures from sample printouts. The overlap between the four spectra is particularly large in the 700-1200 nm range, because the four paints have similar reflection properties in the IR region. Figure 5 also shows the resolution of the underlying interferometer, defined in frequency as $\Delta v = 1.206*c/L$. The limited spectrometer resolution makes it very difficult to get a high spectral resolution measurement of the spectral signatures. Figure 5 is obtained by displacing the PZT as much as possible, correcting for scan distortions, piecing together multiple sections of interferograms and Fourier transforming. Figure 4(b) shows the distance between $I_{x,y}$ and R_1, R_2, and R_3, and Fig. 4(c) shows the result of the ML discrimination. The four shades present the four spectral signatures. ML-TDF determines the correct spectral signature for most of the pixels in the picture. The areas of incorrect decision are caused by noise from either the amplifier or the drift in PZT displacement.
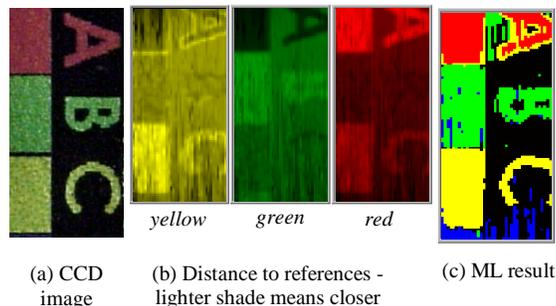

(a) CCD image   (b) Distance to references - lighter shade means closer   (c) ML result

yellow   *green*   *red*

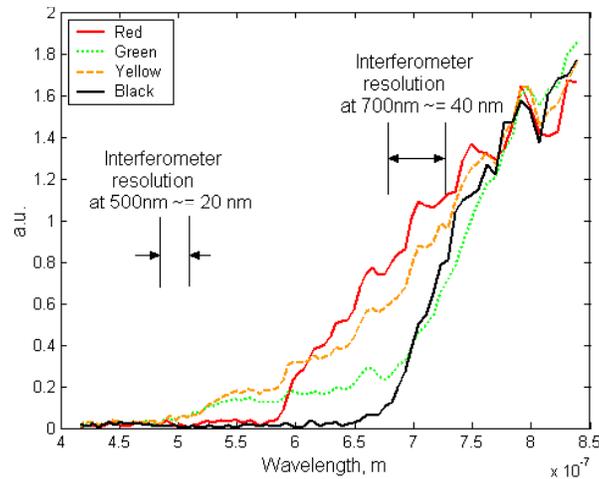Fig. 4. Discrimination of broadband features by TDF-ML.

Fig. 5. Experimental measurement of source spectra.

ML-TDF relies on the distances in *S* to discriminate between highly overlapping spectral signatures. The amount of noise at each pixel determines how close two spectral signatures can be before the probability of correct discrimination between the two drops to unacceptable levels. As discussed in Ref. [4], if the signal to noise ratio is not too low, ML-TDF would allow discrimination of nearly monochromatic signatures with frequency separation below the Rayleigh spectral resolution of the underlying interferometer. From the distance data shown in Fig. 4(b), we can obtain a sample distribution of the distance noise. From the distance noise distribution, we estimated the standard deviation of the white Gaussian noise to be 0.045, normalized to the average measured interferogram power. 99.9 % discrimination accuracy between two nearly monochromatic signatures of equal intensity is theoretically achievable for two sources separated by only 789 cm^{-1} (2 nm around 400 nm).

Many novel miniature imaging spectrometer could potentially be made using microfabrication technology and tightly integrated with integrated circuits, but traditional spectral signature discrimination system designs rule out such devices because of their poor spectral resolution, as well as poor scan linearities in the case of interferometers with micro-electro-mechanical (MEMS) components. Furthermore, simply miniaturizing the imaging spectrometer will leave out the computationally demanding discrimination to another system. TDF and ML-TDF discrimination systems do not need to correct for the scanning nonlinearity or perform Fourier transforms, because the discrimination algorithm does not require linearized spectra in the frequency domain. This significantly reduces data analysis complexity. The architecture is not robust against detector nonlinearities that distort the interferogram amplitude, but, as we have demonstrated, it is robust against scan nonlinearities, which could be much more significant than detector nonlinearities in a MEMs system. TDF and ML-TDF also permit a broad range of spectral sensing devices to be used, not constrained by specific requirements of conventional or Fourier transform spectrometers. Without resorting to computationally demanding discrimination algorithms, we have demonstrated the discrimination of highly overlapping spectral signatures in ML-TDF, and suppression of specific spectral figures. Architectures of TDF and ML-TDF will enable a large variety of miniature spectrometers to perform sophisticated sensing tasks with minimal data processing.